Materials Advances

ROYAL SOCIETY OF CHEMISTRY

PAPER

View Article Online
View Journal | View Issue

Check for updates

Cite this: *Mater. Adv.*, 2022, 3, 3620

Suppression of phosphine-protected Au_9 cluster agglomeration on $SrTiO_3$ particles using a chromium hydroxide layer†

Abdulrahman S. Alotabi, [abc] D. J. Osborn,[d] Shuhei Ozaki,[e] Yuki Kataoka,[e] Yuichi Negishi, [e] Siriluck Tesana,[f] Gregory F. Metha [d] and Gunther G. Andersson *[ac]

Gold clusters have been shown to have great potential for use as co-catalysts in photocatalytic water splitting. Agglomeration of Au clusters deposited onto semiconductor surfaces into larger particles is a major challenge. Metal oxide overlayers can be used to improve the stability of Au clusters on surfaces and avoid their agglomeration. The aim of this work is to investigate the inhibition of phosphine-protected Au_9 clusters beneath a $Cr(OH)_3$ overlayer to agglomerate under conditions of photocatalytic water splitting (*i.e.* UV irradiation). Au_9 was deposited on the surface of $SrTiO_3$ using a solution impregnation method followed by photodeposition of a $Cr(OH)_3$ layer. After UV light irradiation for 7 hours for photocatalytic water splitting, uncovered Au clusters on $SrTiO_3$ agglomerated into larger particles. However, agglomeration was inhibited when a thin $Cr(OH)_3$ layer was deposited onto the $SrTiO_3$-Au_9 system. From careful XPS measurements, the chemical state of the overlayer is initially determined to be $Cr(OH)_3$ but upon heating at 200 °C for 10 min it converts to Cr_2O_3. Through photocatalysis experiments it was found that the $Cr(OH)_3$ overlayer blocks the sites for O evolution reaction on the $SrTiO_3$-Au_9.

Received 22nd December 2021,
Accepted 10th March 2022

DOI: 10.1039/d1ma01226f

rsc.li/materials-advances

Open Access Article. Published on 14 March 2022. Downloaded on 11/19/2024 7:23:42 PM.
This article is licensed under a Creative Commons Attribution-NonCommercial 3.0 Unported Licence.

Introduction

Metal clusters are formed by a specific number of metal atoms and are generally less than 2 nm in size. Metal clusters exhibit unique physical and chemical properties which are different to those of nanoparticles formed by the same element and the respective bulk materials.[1–4] Clusters can be synthesised with protecting ligands to stabilise the cluster core and prevent agglomeration.[5,6] In contrast to gas phase generated clusters, ligand protected clusters can be synthesised on a larger scale. Atomically precise chemically synthesised ligated clusters deposited onto metal oxides are known to be photocatalytically active in water splitting.[2,7,8] When using chemically synthesised ligated clusters, the ligands need to be removed to generate naked clusters on a surface as active sites of a photocatalyst.[9] Au clusters decorated metal oxide surfaces show enhanced photocatalytic water splitting activity due to the size and dispersibility of ultrasmall metal clusters on surfaces.[10–16] However, removal of the ligands of the deposited clusters without causing agglomeration of the clusters is a challenging task.[2,7,17] Agglomeration of the clusters render them inefficient as active sites in photocatalysis, particularly when the catalytic performance is based on the size of the clusters. For example, Au_{25} clusters on $BaLa_4Ti_4O_{15}$ surfaces show a strong decrease in photocatalytic activity if the clusters increase in size.[13] It is also known that Au clusters on surfaces exposed to constant irradiation can result in agglomeration of the clusters.[18,19]

Inhibiting the agglomeration of Au clusters decorated on metal oxide surfaces can be achieved by using surface modification and coating strategies.[20,21] Krishnan *et al.* have stabilised $Au_9(PPh_3)_8(NO_3)_3$ and $Au_{13}(dppe)_5Cl_2Cl_3$ clusters deposited on

[a] *Flinders Institute for Nanoscale Science and Technology, Flinders University, Adelaide, South Australia 5042, Australia*
[b] *Department of Physics, Faculty of Science and Arts in Baljurashi, Albaha University, Baljurashi 65655, Saudi Arabia*
[c] *Flinders Microscopy and Microanalysis, College of Science and Engineering, Flinders University, 5042 Adelaide, Australia*
[d] *Department of Chemistry, University of Adelaide, Adelaide, South Australia 5005, Australia*
[e] *Department of Applied Chemistry, Faculty of Science, Tokyo University of Science, 1-3 Kagurazaka, Shinjuku-ku, Tokyo 162-8601, Japan*
[f] *The MacDiarmid Institute for Advanced Materials and Nanotechnology, School of Physical and Chemical Sciences, University of Canterbury, Christchurch 8141, and National Isotope Centre, GNS Science, Lower Hutt 5010, New Zealand*

† Electronic supplementary information (ESI) available: The HAADF-STEM images of *in situ* STEM measurements of the Au_9 clusters, the details of the XPS 4f Au spectra, their fitting and quantification and results from the water splitting reaction with and without addition of air (oxygen). See DOI: 10.1039/d1ma01226f

© 2022 The Author(s). Published by the Royal Society of Chemistry

Open Access Article. Published on 14 March 2022. Downloaded on 11/19/2024 7:23:42 PM.
This article is licensed under a Creative Commons Attribution-NonCommercial 3.0 Unported Licence.

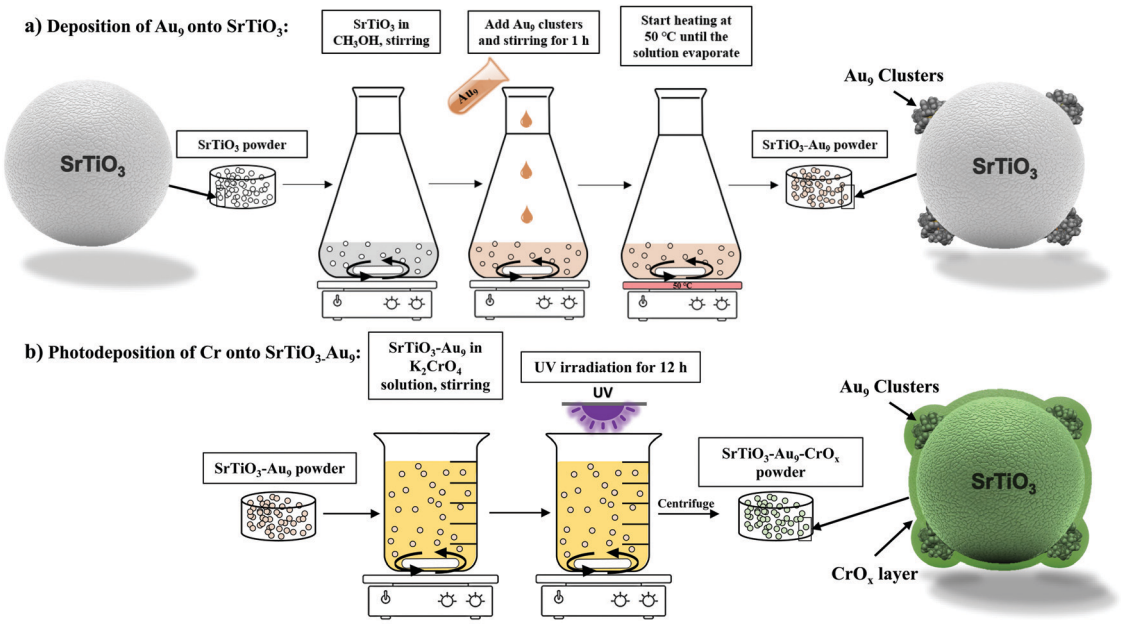

Scheme 1 Experimental procedure of (a) Au_9 deposition on $SrTiO_3$ particles and (b) photodeposition of CrO_x onto $SrTiO_3$-Au_9 particles.

ALD TiO_2 films by pre-treatment of the surface through heating and sputtering to introduce defects.[22,23] These defects sites stabilise the Au clusters against agglomeration on the surface. Recently, Xu *et al.* reported that the photostability of glutathione-protected Au_{25} clusters on SiO_2 spheres was increased by addition of multifunctional branched poly-ethylenimine (BPEI).[24] Subsequent coating with TiO_2 shell produced a photocatalyst with improved efficiency and photostability, even after long periods of light irradiation.

It has been shown that deposition of a CrO_x overlayer can stabilise nanoparticles and clusters. Domen *et al.* have developed a method to improve the stability of rhodium nanoparticles using a CrO_x overlayer.[25–28] CrO_x overlayers also can prevent the back reaction H^+ and O_2 to H_2O (oxygen photoreduction reaction) in photocatalysts used for water splitting,[29–38] with the effectiveness of the overlayer depending on its thickness.[39] CrO_x layers have been applied to a range of co-catalysts deposited on other metal oxide substrates, such as platinum nanoparticles,[38,40] palladium nanoparticles,[41] silver nanoparticles[39] and metal oxides (NiO_x, RuO_2, Rh_2O_3 and CuO_x).[28,42] Overlayers of other metal oxides have also been employed to stabilise co-catalysts and to prevent the back reaction in photocatalysis.[43–46]

Chemically synthesised phosphine-protected Au clusters have attracted much attention because of their fluxional behavior and facile removal of the Au-Ph ligands.[2,21,47] The aim of the present study is to investigate the size of $Au_9(PPh_3)_8(NO_3)_3$ (hereafter referred to as Au_9) deposited onto $SrTiO_3$ nanoparticles before and after the removal of the ligands and after undergoing photocatalysis. This study includes an investigation of the influence of the chromium oxide (CrO_x) layer in preventing cluster agglomeration. CrO_x overlayers are photodeposited, before the removal of the ligands, to inhibit the Au clusters from agglomeration. The size of Au_9 clusters was examined to investigate the effectiveness of the CrO_x overlayer to stabilising phosphine-protected Au clusters after heating and UV irradiation. Finally, the influence of CrO_x coverage for Au_9 deposited onto $SrTiO_3$ on overall photocatalytic water splitting rate is examined.

Experimental methods and techniques

Material and sample preparation

Material. $SrTiO_3$ with a purity of 99% (<100 nm particle size) was purchased from Sigma-Aldrich (Australia). Au_9 was synthesized using the procedure reported earlier.[48] Methanol (CH_3OH) (99.9% super gradient HPLC (ACI labscan)), potassium chromate (K_2CrO_4) (purity ≥99%, Sigma-Aldrich, Australia) and deionised water were used for sample preparation.

Deposition mechanism. Scheme 1 depicts the experimental procedure for preparing (a) the $SrTiO_3$-Au_9 samples and (b) the $SrTiO_3$-Au_9-CrO_x samples *via* impregnation and photodeposition.

(a) Deposition of Au_9 onto $SrTiO_3$ ($SrTiO_3$-Au_9). $SrTiO_3$-Au_9 was prepared using an impregnation method (see Scheme 1a). First, 1 g of $SrTiO_3$ was dispersed in 10 mL of CH_3OH. Subsequently, 10 mL of a Au_9 cluster solution (0.12 mM) was added to a stirred suspension of $SrTiO_3$ (1 g $SrTiO_3$, 10 mL CH_3OH) and left to stir for 1 h at room temperature. The total volume of a CH_3OH solution was 20 mL and concentration of Au_9 in the solution was 0.06 mM. Assuming complete adhesion of the clusters onto the substrate, the total Au content of the $SrTiO_3$-Au_9 sample is 0.2 wt% Au content. The stirred suspension was heated at 50 °C under N_2 flow until the CH_3OH had evaporated (approximately 8–10 min for evaporating the CH_3OH). The $SrTiO_3$-Au_9 powder was collected without further treatment.

© 2022 The Author(s). Published by the Royal Society of Chemistry

Open Access Article. Published on 14 March 2022. Downloaded on 11/19/2024 7:23:42 PM.
This article is licensed under a Creative Commons Attribution-NonCommercial 3.0 Unported Licence.

(b) Photodeposition of Cr onto $SrTiO_3$-Au_9. CrO_x was photodeposited onto the $SrTiO_3$-Au_9 samples to form an overlayer (see Scheme 1b). 500 mg of $SrTiO_3$-Au_9 powder was added to a 0.5 mM aqueous K_2CrO_4 solution (200 mL). The mixture was irradiated for 12 hours using a UV LED source (Vishay, VLMU3510-365-130) while stirring at a speed of 1000 rpm. The radiant power of the UV LED source was 690 mW at a wavelength of 365 nm. After irradiation, the $SrTiO_3$-Au_9-CrO_x powder was collected by centrifugation and washed with deionised water. ICP-MS analysis determined that approximately 20% of all available Cr was deposited onto the $SrTiO_3$-Au_9 particles.

Heat treatment. All samples were heated under vacuum (below 1×10^{-3} mbar) at 200 °C for 10 min to remove the ligands before photocatalytic testing.[49] XPS samples were heated at the same temperature and for the same time; spectra were recorded immediately after heating.

Analytical methods

X-Ray photoelectron spectroscopy (XPS). X-Ray photoelectron spectroscopy (XPS) was used to determine the size of the Au clusters deposited onto the substrate and to determine the surface elemental compositions. XPS was applied using an UHV instrument with a Phoibos 100 hemispherical analyser (SPECS) and a base pressure of a few 10^{-10} mbar with the instrument described in ref. 50 A non-monochromatic X-ray source with a Mg anode (12 kV–200 W, Kα line with an excitation energy of 1253.6 eV) was used for X-ray irradiation. Survey scans at 40 eV at a step size of 0.5 eV were measured first followed by high-resolution scans at a pass energy of 10 eV. The angle between the X-ray source and the analyser is 54.7°. At a pass energy of 10 eV the FWHM of the Ag $3d_{5/2}$ peak is <1 eV. The uncertainty of the peak positions is typically 0.2 eV.

High-resolution XP spectra were recorded for Au 4f, Sr 3d, Cr 2p, Ti 2p, P 2p, O 1s and C 1s. The XP spectra were calibrated using the main carbon peak at 285 eV to correct for charging effects.[51] The peak areas were used to calculate the relative intensities taking into account the transmission function and cross-section.[52]

Scanning transmission electron microscopy (STEM). STEM was applied to determine the size and distribution of the deposited Au clusters and the thickness of the CrO_x overlayer. STEM was applied with a high-angle annular dark-field (HAADF) detector (FEI Titan Themis 80–200). The STEM measurements were operated at 200 kV with a HAADF collection angle greater than 50 mrad. The energy-dispersive X-ray spectroscopy (EDS) elemental maps was employed with STEM-HAADF to determine the elemental distribution. STEM-EDS elemental maps obtained at a magnification up to 5 nm. The Velox™ software was used to process elemental maps data. It should be noted that STEM imaging can alter the samples due to the energy deposited by the electrons impinging on the sample (*vide infra*).

Photocatalytic water splitting reactions

Overall water splitting. The photocatalytic activity was tested using a high-pressure Hg lamp (400 W, main wavelength at 365 nm) within a quartz cell (see Scheme S1, ESI†).[19] The reaction was carried out in a closed gas flow system with Ar flow of 30 mL min^{-1} using a solution containing 500 mg of the photocatalyst (*i.e.* $SrTiO_3$, $SrTiO_3$-Au_9 and $SrTiO_3$-Au_9-CrO_x after heating) with 350 mL of water. Before the photocatalysis experiment, the reaction cell was purged with Ar gas bubbling through the water for 1 h to ensure that air was completely removed from the reaction vessel.

Hydrogen evolution using a sacrificial reagent. This experiment was performed using the same procedure as overall water splitting except that 10% of the water is replaced with methanol.

Oxygen photoreduction reaction. Using the same procedure as hydrogen evolution with the sacrificial reagent, oxygen was introduced into the reaction with a closed gas flow system using a 7 : 3 mixture of Ar to air at a flow rate of 30 mL min^{-1}.

Results and discussion

Before heating

Characterisation of $SrTiO_3$-Au_9 and $SrTiO_3$-Au_9-CrO_x. The size of phosphine-protected Au_9 clusters deposited onto $SrTiO_3$ particles is examined in this work, along with the effect of the CrO_x overlayer on the size of Au_9 clusters, using XPS. (It should be noted that the coating is labelled "CrO_x" until we confirm the nature of the Cr component (*vide infra*)). The XPS Au spectra of $SrTiO_3$-Au_9 and $SrTiO_3$-Au_9-CrO_x are shown in Fig. 1.

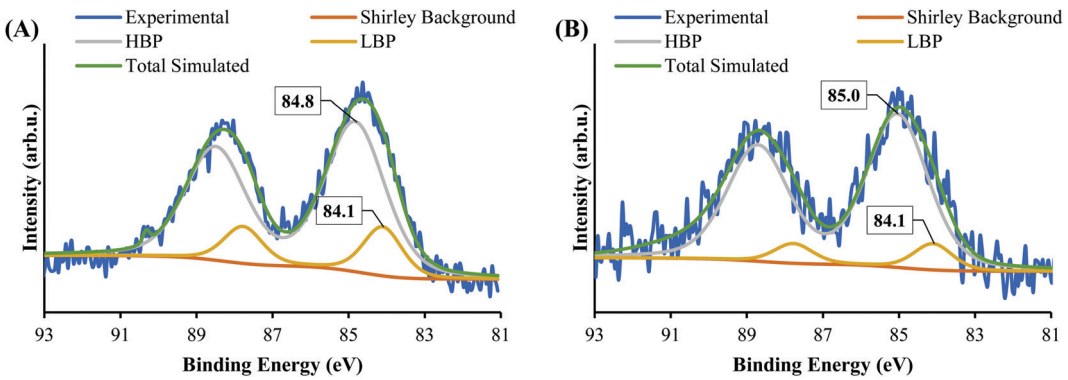

Fig. 1 XPS spectra of Au 4f of (A) Au_9 deposited on $SrTiO_3$ and (B) $SrTiO_3$-Au_9 after photodeposition of a CrO_x layer.

© 2022 The Author(s). Published by the Royal Society of Chemistry

Open Access Article. Published on 14 March 2022. Downloaded on 11/19/2024 7:23:42 PM.
This article is licensed under a Creative Commons Attribution-NonCommercial 3.0 Unported Licence.

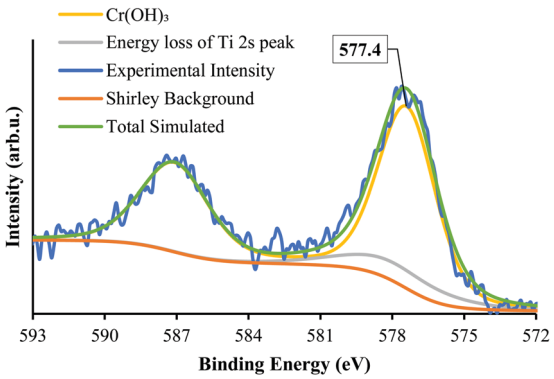

Fig. 2 XPS Cr 2p spectrum of $SrTiO_3$-Au_9 after photodeposition of a CrO_x layer.

A summary of the Au 4f peak positions and full-width-half-maximum (FWHM) is presented in Table S1 (ESI†) and full elemental composition analyses and peak positions are presented in Tables S2 and S3 (ESI†). In the present experiment, the Au 4f spectra were fitted with two doublet peaks (in addition to the spin–orbit $4f_{7/2}$ and $4f_{5/2}$ pairs). These peaks are referred to as the 'high binding peak' (HBP) and 'low binding peak' (LBP), as described in our previous work.[49] The position of the Au $4f_{7/2}$ HBP is observed at 84.8–85 eV (FWHM of 1.7 ± 0.2 eV) while the Au $4f_{7/2}$ LBP is at 84.1 eV (FWHM of 1.2 ± 0.2 eV). Through the XPS final state effect, the size of the phosphine-protected Au_9 clusters can be determined using the Au $4f_{7/2}$ peak position and the FWHM.[23,53–57] The peak position of phosphine-protected Au_9 clusters is known to be 84.8–85.2 eV, with a typical FWHM of 1.7 ± 0.2 eV. The peak position for agglomerated Au_9 clusters shifts to 83.7–84.1 eV with FWHM of 1.0 ± 0.2 eV.[23,53–57] The Au 4f spectrum of $SrTiO_3$-Au_9 shows 83% of the intensity at the HBP position, corresponding to non-agglomerated Au_9 clusters, and 17% at the LBP, corresponding to agglomerated Au_9 clusters. The $SrTiO_3$-Au_9-CrO_x shows 90% of the Au 4f spectrum intensity at the HBP position and 10% at the LBP position. The LBP of $SrTiO_3$-Au_9 has a slightly higher percentage than $SrTiO_3$-Au_9-CrO_x, which can be attributed to a somewhat higher degree of agglomeration of the Au_9 clusters in $SrTiO_3$-Au_9 without a CrO_x layer. However, more than 80% of the Au 4f intensity for both samples are at the HBP, indicating that most of the Au_9 clusters remain non-agglomerated. It is important to note that the triphenylphosphine (PPh_3) ligands are difficult to determine using XPS due to the overlapping energies of P 2p and Sr 3d peaks (see Fig. S1, ESI†).[58]

The state of Cr photodeposited on $SrTiO_3$-Au_9 was investigated using XPS. Fig. 2 shows the Cr 2p spectrum of

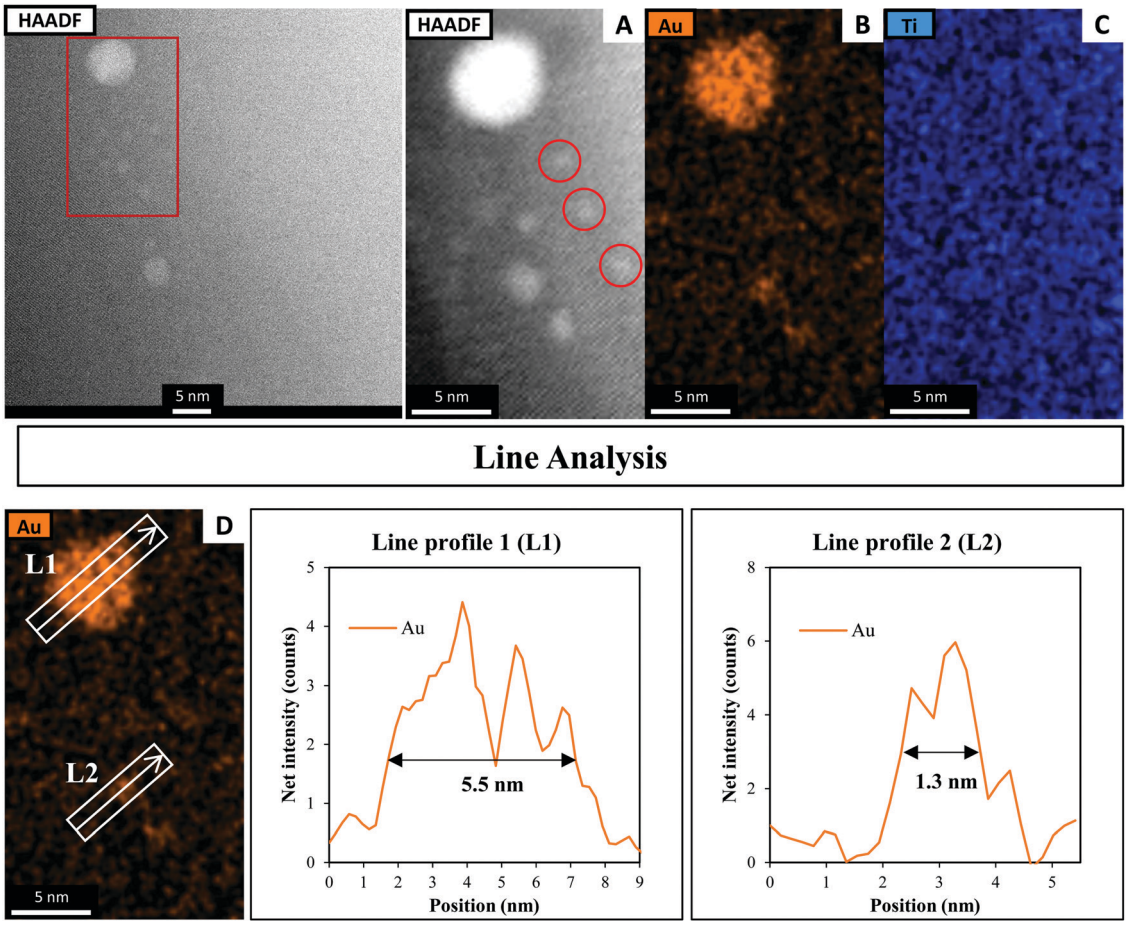

Fig. 3 (A) HAADF-STEM image with EDX elemental mapping of (B) Au and (C) Ti in $SrTiO_3$-Au_9 before heating and (D) line analyses of the Au signal.

Open Access Article. Published on 14 March 2022. Downloaded on 11/19/2024 7:23:42 PM.
This article is licensed under a Creative Commons Attribution-NonCommercial 3.0 Unported Licence.

$SrTiO_3$-Au_9-CrO_x before heating. The Cr 2p spectrum was fitted with a single doublet peak ($2p_{3/2}$ and $2p_{1/2}$). It was fitted by including the Ti 2s energy loss peak, which occurs in the same energy region. In our previous work, the Cr 2p peak was described and fitted using a fixed relation between the intensity of the Ti $2p_{3/2}$ and the Ti 2s loss peak.[59] The Cr $2p_{3/2}$ peak is found at 577.4 ± 0.2 eV, which can be identified from literature reference data as being $Cr(OH)_3$.[60] It should be noted that this is different to the binding energy of Cr_2O_3 and will be discussed below (*vide infra*).

Fig. 3 shows the HAADF-STEM image of Au_9 deposited onto the surface of $SrTiO_3$. The figure includes EDX elemental mapping of Au and Ti as well as line analysis of Au. It should be noted that P was difficult to analyse using STEM-EDX due to the intensity of P in EDX being significantly lower than that of Au and due to overlapping of the P K_α and Au M_α peaks.[61] In Fig. 3A, the HAADF-STEM image shows small bright particles, which can be identified from the EDX mapping as Au features. The line analysis of L1 and L2 confirmed the size of Au features as approximately 5.5 and 1.3 nm, respectively. The HAADF-STEM image shows further small Au clusters, indicated with red circles, that were not detected clearly by EDX mapping (see Fig. 3A). A possible reason for this is that EDX is not suitable for size analysis due to its lower spatial resolution compared with STEM. The size of these Au clusters in the HAADF image is approximately 0.7–0.9 nm. Previous studies

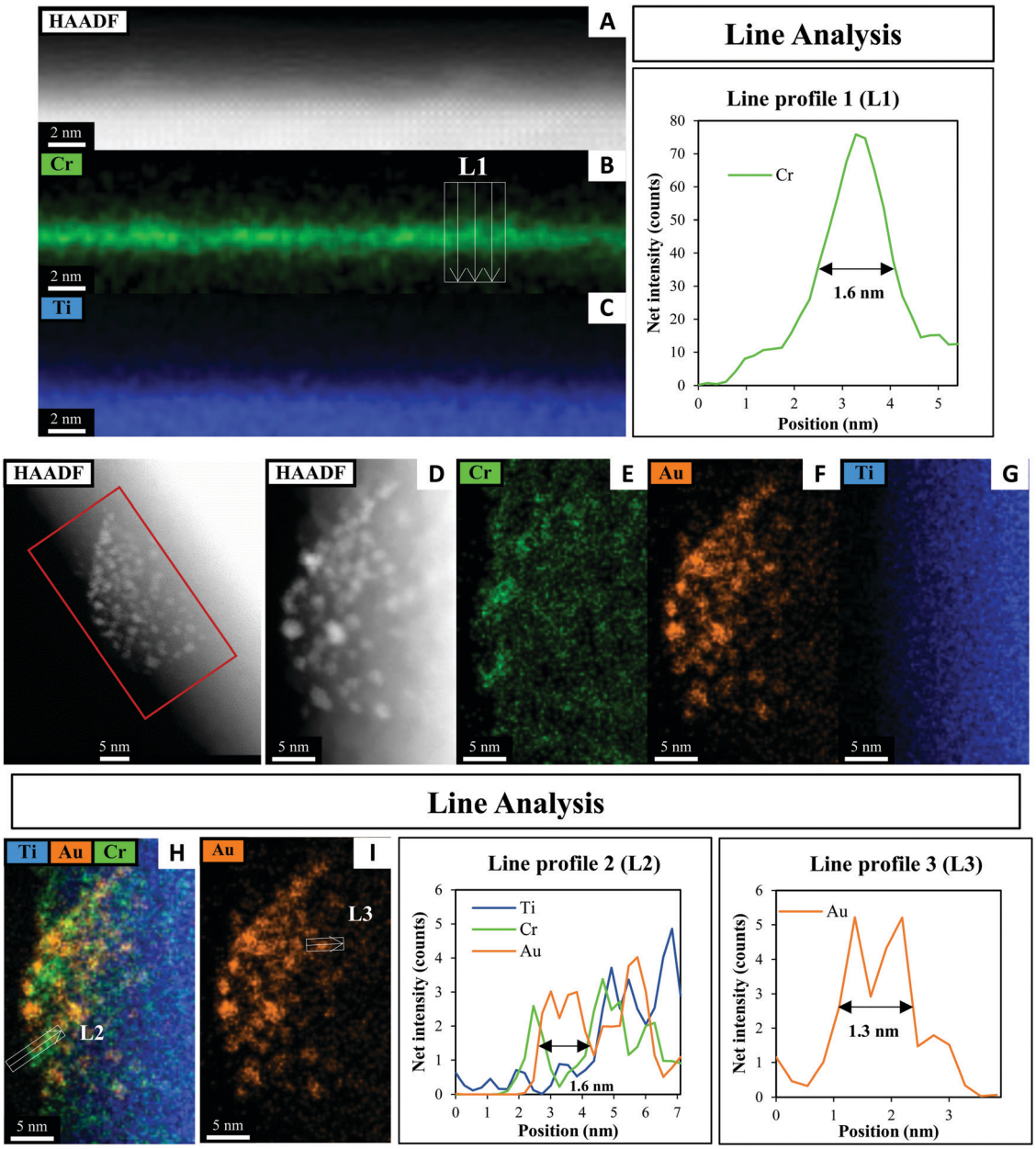

Fig. 4 HAADF-STEM image with EDX elemental mapping and line analyses of the Cr, Au and Ti in $SrTiO_3$-Au_9-$Cr(OH)_3$.

© 2022 The Author(s). Published by the Royal Society of Chemistry

Open Access Article. Published on 14 March 2022. Downloaded on 11/19/2024 7:23:42 PM.
This article is licensed under a Creative Commons Attribution-NonCommercial 3.0 Unported Licence.

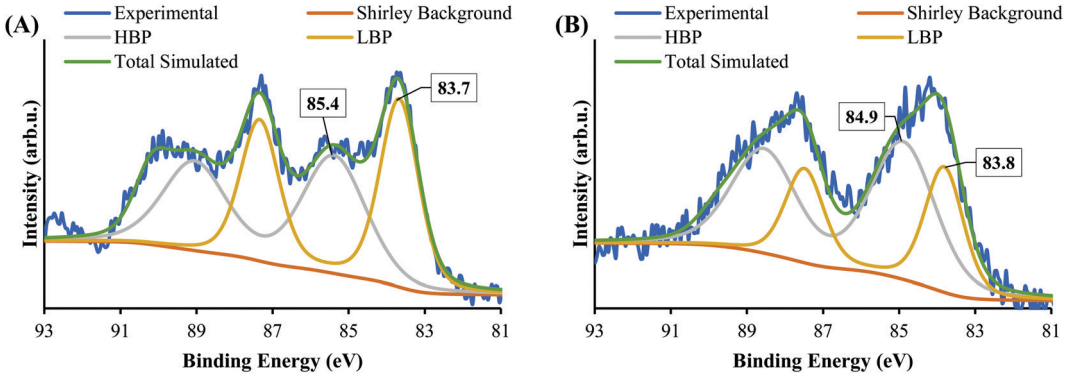

Fig. 5 XPS spectra of Au 4f after heating of (A) $SrTiO_3$-Au_9 and (B) $SrTiO_3$-Au_9-CrO_x.

have shown that the size of a single Au_9 cluster is approximately 0.6 ± 0.2 nm.[56] In the present experiment, the small Au clusters (0.7–0.9 nm) in the HAADF-STEM image are of a similar size as Au_9. Therefore, we conclude that these are non-agglomerated clusters. The Au feature from the STEM-EDX line analysis (Fig. 3L1), which is 5.5 nm in size, is due to many adjacent Au_9 clusters or agglomerations of Au clusters. The Au feature from L2 is 1.3 nm in size, suggesting two adjacent clusters or an agglomeration of two clusters due to the effect of the high-energy STEM electron beam (see Fig. S2, ESI† for more information). This finding is in line with the XPS data that suggested some of the Au clusters had agglomerated on $SrTiO_3$-Au_9 STEM shows the Au cluster sizes for only a small selected area of the sample, which could also be subject to electron beam damage of the clusters. Therefore, the XPS data is considered as being more accurate in identifying the fraction of agglomerated and non-agglomerated clusters because XPS averages over a significant larger number of Au cluster compared to STEM and also because XPS does not cause damage to the clusters resulting in their agglomeration.[53,54] XPS shows that 83% of Au clusters remain non-agglomerated.

A HAADF-STEM image of $SrTiO_3$-Au_9-$Cr(OH)_3$ with EDX elemental mapping and a line analysis of Cr, Au and Ti is shown in Fig. 4. Fig. 4A–C shows the first STEM mapping region which is focused on the edge of $SrTiO_3$-Au_9-$Cr(OH)_3$ to determine the thickness and distribution of $Cr(OH)_3$ at the surface of $SrTiO_3$. The STEM-EDX elemental map L1 at the edge of the $SrTiO_3$-Au_9-$Cr(OH)_3$ shows that the $Cr(OH)_3$ layer is distributed over the entire $SrTiO_3$ surface (Fig. 4B) and has a thickness of 1.6 nm (Fig. 4L1). The line analysis of Cr, Ti and Au (L2) shows that the presence of $Cr(OH)_3$ around the Au clusters (Fig. 4L2). Using the line analysis of L2 and L3 in Fig. 4, the Au clusters are shown to be approximately 1.3–1.6 nm in diameter. This is similar to the size of the Au clusters determined for $SrTiO_3$-Au_9 (*i.e.* without the $Cr(OH)_3$ covering layer, Fig. 3). Note that the STEM-EDX mapping shows Au features with a larger diameter compared to a single Au_9 cluster. Here, the increase in the size of the Au clusters is most likely due to the effect of the high-energy STEM electron beam, (see Fig. S2, ESI† for further information). Again, XPS is considered to be the more accurate method for determining the extent of cluster agglomeration, which was determined to be 90% of Au clusters remain non-agglomerated on $SrTiO_3$ with $Cr(OH)_3$ coverage.

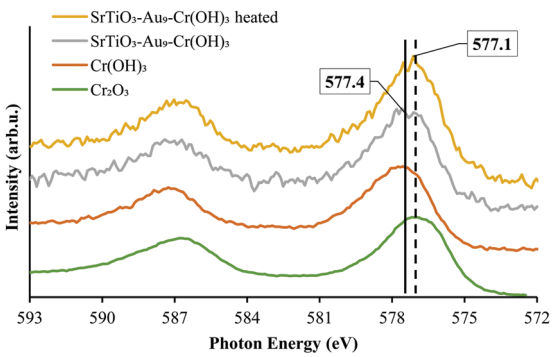

Fig. 6 XPS spectra of Cr 2p of $SrTiO_3$-Au_9-$Cr(OH)_3$ before heating and $SrTiO_3$-Au_9-CrO_x after heating with reference spectrum of Cr_2O_3 and $Cr(OH)_3$ (Fig. S4, ESI† shows complete fitting to all components).

After heating

Fig. 5 shows the XPS Au 4f spectra of $SrTiO_3$-Au_9 and $SrTiO_3$-Au_9-CrO_x after heating (the CrO_x notation is used again here because heating could change the chemical state of the Cr). The Au 4f spectra are again fitted with a HBP and LBP doublet. The peak positions and FWHM are summarised in Table S1 (ESI†). As mentioned above, it is difficult to determine the state of PPh_3 ligands on $SrTiO_3$ using XPS, however, previous studies showed that PPh_3-ligated Au_9 clusters are removed by heating at 200 °C for 10 min.[23,49,53–57] As shown in Fig. 5A, the Au 4f spectrum for $SrTiO_3$-Au_9 after heating is fitted with 50% Au clusters at HBP (85.4 ± 0.2 eV, FWHM of 2.0 ± 0.2 eV) and 50% agglomerated clusters at LBP (83.7 ± 0.2 eV, FWHM of 1.2 ± 0.2 eV). The feature at 89.9 ± 0.2 eV corresponds to Ba $4d_{5/2}$ due to contamination of the commercial $SrTiO_3$ (see Fig. S3, ESI†). After application of the CrO_x overlayer and heating, the Au 4f spectrum for $SrTiO_3$-Au_9-CrO_x is fitted with 65% and 35% of the Au intensity at the HBP (84.9 ± 0.2 eV, FWHM of 2.0 ± 0.2 eV) and LBP (83.8 ± 0.2 eV, FWHM of 1.2 ± 0.2 eV), respectively (see in Fig. 5B). Thus, the comparison of the XPS results between the heated $SrTiO_3$-Au_9 and $SrTiO_3$-Au_9-CrO_x samples indicated that the photodeposition of CrO_x improves the stability of the

Open Access Article. Published on 14 March 2022. Downloaded on 11/19/2024 7:23:42 PM.
This article is licensed under a Creative Commons Attribution-NonCommercial 3.0 Unported Licence.

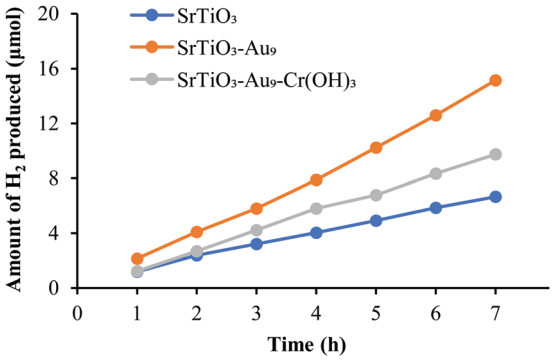

Fig. 7 H_2 evolution by overall photocatalytic water splitting of $SrTiO_3$, $SrTiO_3$-Au_9 and $SrTiO_3$-Au_9-Cr_2O_3 (*i.e.* after heating to remove the ligands).

phosphine-protected Au_9 clusters, with the majority retaining their size after removal of the ligands through heating to 200 °C.

XPS Cr 2p spectra of $SrTiO_3$-Au_9-$Cr(OH)_3$ before and $SrTiO_3$-Au_9-CrO_x after heating are shown in Fig. 6, along with reference spectra for Cr_2O_3 and $Cr(OH)_3$. A summary of the Cr $2p_{3/2}$ peak positions is presented in Table S4 (ESI†). The Cr $2p_{3/2}$ peak for $SrTiO_3$-Au_9-CrO_x after heating shifts slightly to a low binding energy of 577.1 ± 0.2 eV (Fig. S4, ESI†), corresponding to Cr_2O_3.[62] This confirms that a reduction of the $Cr(OH)_3$ layer to Cr_2O_3 occurs by heating. This finding is in agreement with a previous report that heating reduces photodeposited $Cr(OH)_3$ layer to Cr_2O_3.[16]

Photocatalytic water splitting of $SrTiO_3$-Au_9 and $SrTiO_3$-Au_9-Cr_2O_3. Fig. 7 shows the H_2 production by overall water splitting of $SrTiO_3$, $SrTiO_3$-Au_9 and $SrTiO_3$-Au_9-Cr_2O_3 (*i.e.* after heating at 200 °C for 10 min to remove the ligands) over a period of seven hours. Note that the O_2 production is not shown due to the very low O_2 production. This suggests that another oxidation reaction is occurring more readily than OH^- to O_2. One possible reaction is the oxidation of residual PPh_3 ligands on the catalyst surface. Another possibility could be the oxidation of adventitious hydrocarbons absorbed onto the surface when the catalyst is exposed to atmosphere. The H_2 production of $SrTiO_3$-Au_9 is observed to be more than two times higher compared with that of $SrTiO_3$ during the 7 h irradiation period. Surprisingly, $SrTiO_3$-Au_9-Cr_2O_3 shows decreased H_2 production compared to $SrTiO_3$-Au_9 but is higher than $SrTiO_3$. In order to better understand the effect of the overlayer, hydrogen evolution using methanol as a sacrificial reagent was performed with and without air (oxygen) in the reaction system to investigate the role of the back reaction (oxygen photoreduction reaction). Fig. S5, ESI† shows that the $SrTiO_3$ and $SrTiO_3$-Au_9 samples suffer a large drop in H_2 production after O_2 was introduced into the reaction but not the $SrTiO_3$-Au_9-Cr_2O_3 sample. The drop in H_2 production is due to the oxygen photoreduction reaction occurring at the surface of the cocatalyst. This indicates that the back reaction is suppressed with the Cr_2O_3 overlayer for $SrTiO_3$-Au_9-Cr_2O_3.

While the addition of a CrO_x overlayer is expected to increase the H_2 production rate for the overall water splitting reaction due to blocking the back reaction,[29–38] there is a possibility for the observed decrease in H_2 production rate due to an even distribution and a too thick Cr_2O_3 overlayer on the surface of the photocatalyst ($SrTiO_3$). STEM images shows that Cr_2O_3 is deposited in a homogeneous layer with a thickness of *ca.* 1.6 nm across the catalyst (Fig. 4). Having a uniform and too thick Cr_2O_3 layer covering the entire surface could result in stopping the oxidation reaction to occur through blocking the respective sites on the catalyst surface, which blocks the overall water splitting reaction. Kurashige *et al.* noted a similar result in their study of an Au_{25}-CrO_x-$BaLa_4Ti_4O_{15}$ system in which CrO_x was deposited at various concentrations (0.1–1.5 wt%).[19] The authors found that higher Cr contents led to an increase in the coverage and thickness of the CrO_x layer (1.2–2.0 nm), which significantly decreased the water splitting rate. In the above-mentioned studies, this decrease in activity was assumed to be due to a reduction in the numbers of O_2 generation sites.[19] This shows that the amount of CrO_x deposited impacts here the O reduction sites rather the H evolution sites.

After photocatalysis

Determination of Au_9 size after photocatalysis and the influence of the CrO_x layer on agglomeration. Fig. 8 shows the XP Au 4f spectra of $SrTiO_3$-Au_9 and $SrTiO_3$-Au_9-CrO_x after 7 h irradiation during the water splitting reaction (the CrO_x notation

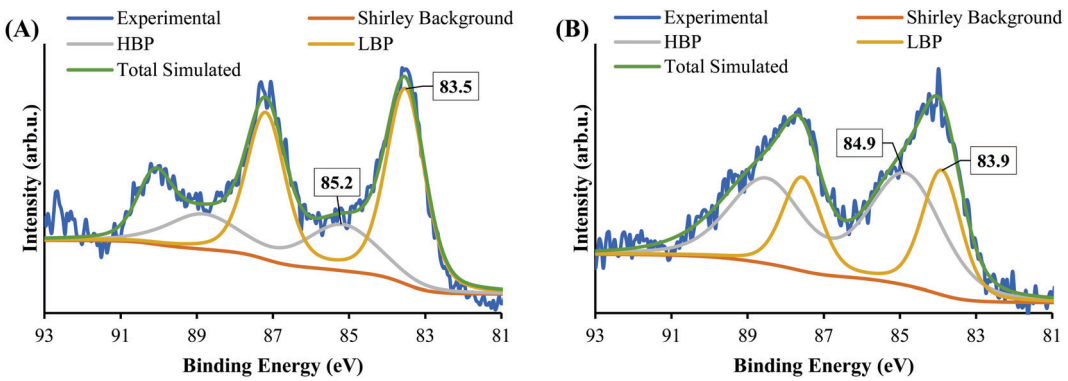

Fig. 8 XPS spectra of Au 4f after 7 h irradiation of (A) $SrTiO_3$-Au_9 and (B) $SrTiO_3$-Au_9-CrO_x.

© 2022 The Author(s). Published by the Royal Society of Chemistry

Open Access Article. Published on 14 March 2022. Downloaded on 11/19/2024 7:23:42 PM.
This article is licensed under a Creative Commons Attribution-NonCommercial 3.0 Unported Licence.

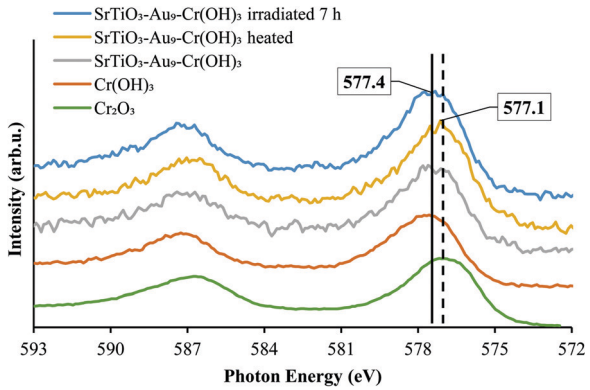

Fig. 9 XPS spectra of Cr 2p of $SrTiO_3$-Au_9-$Cr(OH)_3$ before heating, $SrTiO_3$-Au_9-Cr_2O_3 after heating and $SrTiO_3$-Au_9-CrOx after 7 h irradiation with reference spectrum of Cr_2O_3 and $Cr(OH)_3$ (Fig. S7, ESI† shows complete fitting to all components).

is used again here because photocatalysis could change the chemical state of the Cr). A summary of the peak positions and FWHM is presented in Table S1 (ESI†). After 7 h irradiation, the spectrum of $SrTiO_3$-Au_9 (Fig. 8A) shows that 30% of the Au 4f spectrum is at the HBP position (non-agglomerated clusters), and 70% is at the LBP position (agglomerated clusters). The Ba $4d_{5/2}$ peak appears at 89.9 ± 0.2 eV corresponding to the commercial contamination of $SrTiO_3$ (see Fig. S3, ESI†). The spectrum of $SrTiO_3$-Au_9-CrO_x after 7 h irradiation (Fig. 8B) was fitted with 63% non-agglomerated Au clusters at the HBP and 37% agglomerated Au clusters at the LBP, which is almost the same as after heating (see Fig. 5B). Thus, the comparison of the XPS results between the $SrTiO_3$-Au_9 and $SrTiO_3$-Au_9-CrO_x indicated that the photodeposition of CrO_x significantly improves the stability of the phosphine-protected Au_9 clusters and retains their size after 7 h of water splitting reaction with 10% methanol as a sacrificial reagent (see Fig. S6, ESI† for additional spectra).

XPS Cr 2p spectra of $SrTiO_3$-Au_9-CrO_x before and after heating and after 7 h irradiation, with reference spectra of Cr_2O_3 and $Cr(OH)_3$, are shown in Fig. 9 and summarised in Table S4 (ESI†). After 7 h irradiation, the Cr $2p_{3/2}$ peak for $SrTiO_3$-Au_9-CrO_x appears at 577.4 ± 0.2 eV (Fig. S7, ESI†), corresponding to $Cr(OH)_3$, indicating that the Cr layer converts back to $Cr(OH)_3$ during photocatalysis.[16]

A HAADF-STEM image of $SrTiO_3$-Au_9 after 7 h irradiation with EDX elemental mapping of Au and Ti is shown in Fig. 10 (and summarised in Table S1, ESI†). The image shows that the Au_9 clusters have agglomerated into large particles after 7 h irradiation with no Au clusters left on the surface. The line analysis of Au particles (L1 and L2) confirmed the size of Au particles as approximately 3.9–4.6 nm, with some Au particles

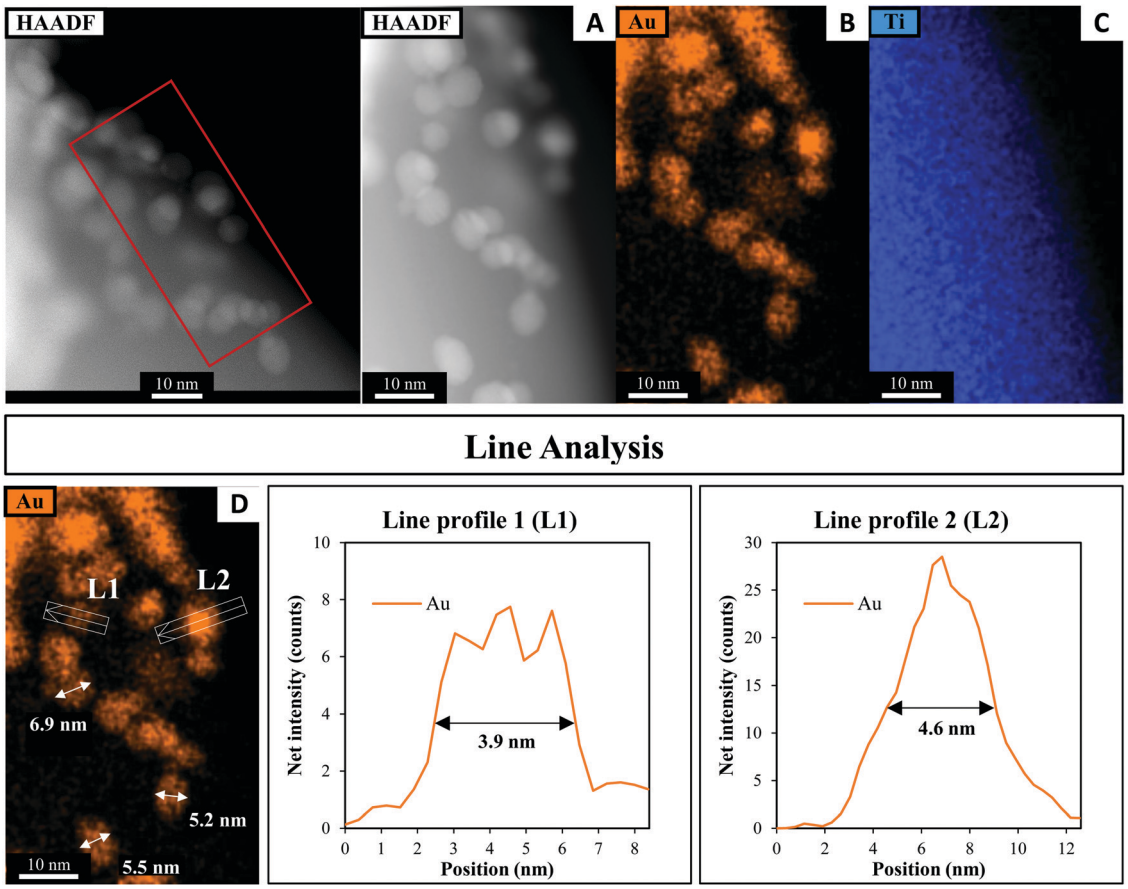

Fig. 10 (A) HAADF-STEM image with EDX elemental mapping of (B) Au and (C) Ti in $SrTiO_3$-Au_9 after 7 h irradiation and (D) line analyses of the Au signal.

Open Access Article. Published on 14 March 2022. Downloaded on 11/19/2024 7:23:42 PM.
This article is licensed under a Creative Commons Attribution-NonCommercial 3.0 Unported Licence.

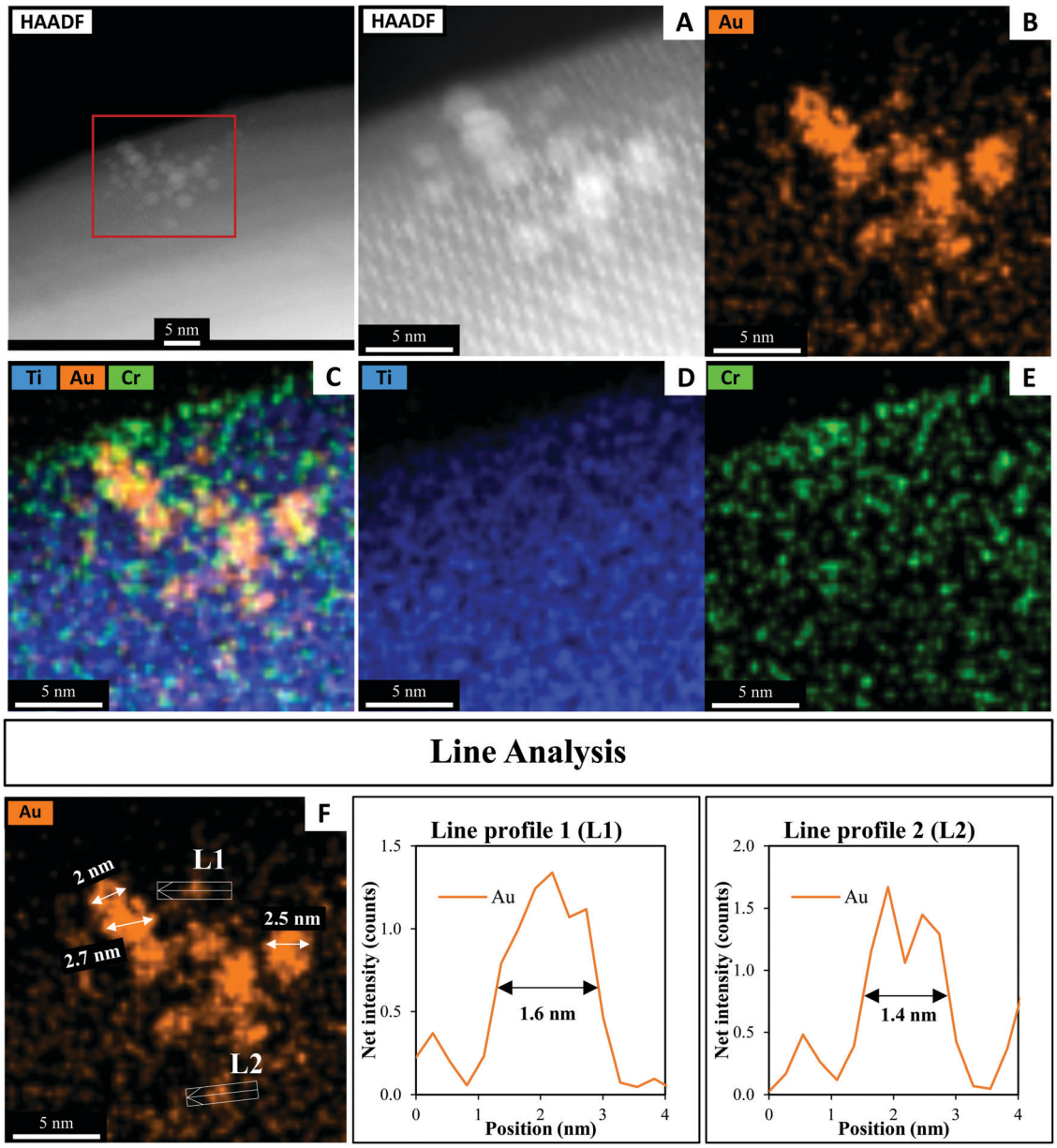

Fig. 11 (A) HAADF-STEM image with EDX elemental mapping of (B) Au, (C) Ti. Au and Cr, (D) Ti and (E) Cr in $SrTiO_3$-Au_9-$Cr(OH)_3$ after 7 h irradiation and (F) line analyses of the Au signal.

having a size of 5.0–6.9 nm (as indicated with arrows in Fig. 10D).

A HAADF-STEM image of $SrTiO_3$-Au_9-$Cr(OH)_3$ after 7 h irradiation with EDX elemental mapping of Au, Cr and Ti is presented in Fig. 11. The typical size of the Au clusters as determined using line analysis (L1 and L2) range from 1.4 to 1.6 nm. This size is nearly identical to Au clusters determined before heating and photocatalysis irradiation (Fig. 4 and Fig. S8, ESI†). Note that STEM-EDX elemental mapping shows that some Au features are 2–2.7 nm in size. As discussed above, the slight increase in the size of the Au clusters is assumed to be caused either by adjacent clusters or agglomeration of Au_9 clusters due to the effect of the STEM electron beam (this is further discussed around Fig. S2, ESI†). As outlined above, XPS is averaged over a significant larger number of Au clusters and is thus considered as being a more representative analysis whereas STEM is averaged over a small selected area of the sample and also causes beam damage. Through XPS analysis it is shown that 63% of Au clusters remain non-agglomerated (Fig. 8B and Table S1, ESI†).

Conclusions

We have demonstrated that application of a $Cr(OH)_3$ overlayer before heating and photocatalytic reaction protects the phosphine-ligated Au_9 clusters from agglomeration after the removal of the ligands. The photocatalytic activity of Au clusters

© 2022 The Author(s). Published by the Royal Society of Chemistry

Open Access Article. Published on 14 March 2022. Downloaded on 11/19/2024 7:23:42 PM.
This article is licensed under a Creative Commons Attribution-NonCommercial 3.0 Unported Licence.

deposited on $SrTiO_3$ was investigated as well as the influence of the addition of a Cr_2O_3 overlayer. For $SrTiO_3$-Au_9, the Au clusters agglomerated, forming large particles (up to 8 nm in size) after the overall photocatalytic water splitting reaction. The results show that only 30% of the Au clusters remain non-agglomerated on the $SrTiO_3$ surface after 7 h irradiation. When a $Cr(OH)_3$ overlayer was added, more than 60% Au clusters on the surface of $SrTiO_3$ remained non-agglomerated after heating and with 7 h of photocatalytic water splitting under UV irradiation. The $Cr(OH)_3$ layer was converted to Cr_2O_3 upon heating and was found to be returned to $Cr(OH)_3$ after photocatalytic water splitting. The H_2 production rate reduced after photodeposition of a $Cr(OH)_3$ layer. It is assumed that the decrease of the H_2 production is due to the even distribution and thickness of the Cr_2O_3 layer on the surface of the semiconductor photocatalyst, blocking the O_2 generating sites then leading to a decrease of the overall photocatalytic water splitting reaction. Although the deposition of a $Cr(OH)_3$ protective layer has been demonstrated for Au_9 clusters deposited onto a $SrTiO_3$ substrate, this approach could be applied to other sized Au clusters on other metal oxide substrates.

Data availability statement

The data that support the findings of this study are available from the corresponding author upon reasonable request.

Conflicts of interest

There are no conflicts to declare.

Acknowledgements

Part of this research was undertaken on the soft X-ray spectroscopy beamline at the Australian Synchrotron, Victoria, Australia (AS1/SXR/15819). We would like to thank Dr Bruce Cowie from the Australian Synchrotron for his assistance. The work is supported by the US army project FA5209-16-R-0017. This research was performed as part of the Australian Solar Thermal Research Institute (ASTRI), a project supported by the Australian Government, through the Australian Renewable Energy Agency (ARENA). Abdulrahman Alotabi acknowledges Albaha University for providing scholarship support. The authors acknowledge the facilities, and the scientific and technical assistance, of Microscopy Australia (formerly known as AMMRF) and the Australian National Fabrication Facility (ANFF) at Flinders University. The authors acknowledge Flinders Microscopy and Microanalysis and their expertise. We thank Dr Ashley Slattery from Adelaide Microscopy for the STEM measurements and A/Prof Vladimir Golovko (Canterbury University) for providing the $Au_9(PPh_3)_8(NO_3)_3$ clusters.

References

1 V. Borman, M. Pushkin, V. Tronin and V. Troyan, *J. Exp. Theor. Phys.*, 2010, **110**, 1005–1025.
2 V. Sudheeshkumar, K. O. Sulaiman and R. W. J. Scott, *Nanoscale Adv.*, 2020, **2**, 55–69.
3 R. Jin, *Nanoscale*, 2010, **2**, 343–362.
4 T. Castro, R. Reifenberger, E. Choi and R. P. Andres, *Phys. Rev. B: Condens. Matter Mater. Phys.*, 1990, **42**, 8548–8556.
5 R. Jin, C. Zeng, M. Zhou and Y. Chen, *Chem. Rev.*, 2016, **116**, 10346–10413.
6 L. Liu and A. Corma, *Chem. Rev.*, 2018, **118**, 4981–5079.
7 L. Howard-Fabretto and G. G. Andersson, *Adv. Mater.*, 2020, **32**, 1904122.
8 A. Alarawi, V. Ramalingam and J.-H. He, *Mater. Today Energy*, 2019, **11**, 1–23.
9 W. Kurashige, Y. Mori, S. Ozaki, M. Kawachi, S. Hossain, T. Kawawaki, C. J. Shearer, A. Iwase, G. F. Metha, S. Yamazoe, A. Kudo and Y. Negishi, *Angew. Chem., Int. Ed.*, 2020, **59**, 7076–7082.
10 S. Yang, S. Ding, C. Zhao, S. Huo, F. Yu, J. Fang and Y. Yang, *J. Mater. Sci.*, 2021, **56**, 13736–13751.
11 C. Wang, P. Lv, D. Xue, Y. Cai, X. Yan, L. Xu, J. Fang and Y. Yang, *ACS Sustainable Chem. Eng.*, 2018, **6**, 8447–8457.
12 W. Kurashige, Y. Niihori, S. Sharma and Y. Negishi, *Coord. Chem. Rev.*, 2016, **320-321**, 238–250.
13 Y. Negishi, M. Mizuno, M. Hirayama, M. Omatoi, T. Takayama, A. Iwase and A. Kudo, *Nanoscale*, 2013, **5**, 7188–7192.
14 Y. Negishi, Y. Matsuura, R. Tomizawa, W. Kurashige, Y. Niihori, T. Takayama, A. Iwase and A. Kudo, *J. Phys. Chem. C*, 2015, **119**, 11224–11232.
15 W. Kurashige, R. Hayashi, K. Wakamatsu, Y. Kataoka, S. Hossain, A. Iwase, A. Kudo, S. Yamazoe and Y. Negishi, *ACS Appl. Energy Mater.*, 2019, **2**, 4175–4187.
16 T. Kawawaki, Y. Kataoka, M. Hirata, Y. Akinaga, R. Takahata, K. Wakamatsu, Y. Fujiki, M. Kataoka, S. Kikkawa, A. S. Alotabi, S. Hossain, D. J. Osborn, T. Teranishi, G. G. Andersson, G. F. Metha, S. Yamazoe and Y. Negishi, *Angew. Chem., Int. Ed.*, 2021, **60**, 21340–21350.
17 G. G. Andersson, V. B. Golovko, J. F. Alvino, T. Bennett, O. Wrede, S. M. Mejia, H. S. Al Qahtani, R. Adnan, N. Gunby and D. P. Anderson, *J. Chem. Phys.*, 2014, **141**, 014702.
18 W. Kurashige, R. Kumazawa, Y. Mori and Y. Negishi, *J. Mater. Appl.*, 2018, **7**, 1–11.
19 W. Kurashige, R. Kumazawa, D. Ishii, R. Hayashi, Y. Niihori, S. Hossain, L. V. Nair, T. Takayama, A. Iwase, S. Yamazoe, T. Tsukuda, A. Kudo and Y. Negishi, *J. Phys. Chem. C*, 2018, **122**, 13669–13681.
20 C.-L. Tan, F. Zhang, Y.-H. Li, Z.-R. Tang and Y.-J. Xu, *Res. Chem. Intermed.*, 2021, **47**, 29–50.
21 R. M. Adnan, M. Jenica, A. S. Alotabi, G. F. Metha and G. G. Andersson, *Adv. Sci.*, 2022, DOI: 10.1002/advs.202105692.
22 G. Krishnan, N. Eom, R. M. Kirk, V. B. Golovko, G. F. Metha and G. G. Andersson, *J. Phys. Chem. C*, 2019, **123**, 6642–6649.
23 G. Krishnan, H. S. Al Qahtani, J. Li, Y. Yin, N. Eom, V. B. Golovko, G. F. Metha and G. G. Andersson, *J. Phys. Chem. C*, 2017, **121**, 28007–28016.

Open Access Article. Published on 14 March 2022. Downloaded on 11/19/2024 7:23:42 PM.
This article is licensed under a Creative Commons Attribution-NonCommercial 3.0 Unported Licence.

24 B. Weng, K.-Q. Lu, Z. Tang, H. M. Chen and Y.-J. Xu, *Nat. Commun.*, 2018, **9**, 1543.
25 K. Maeda, K. Teramura, D. Lu, N. Saito, Y. Inoue and K. Domen, *J. Phys. Chem. C*, 2007, **111**, 7554–7560.
26 N. Sakamoto, H. Ohtsuka, T. Ikeda, K. Maeda, D. Lu, M. Kanehara, K. Teramura, T. Teranishi and K. Domen, *Nanoscale*, 2009, **1**, 106–109.
27 M. Yoshida, K. Takanabe, K. Maeda, A. Ishikawa, J. Kubota, Y. Sakata, Y. Ikezawa and K. Domen, *J. Phys. Chem. C*, 2009, **113**, 10151–10157.
28 K. Maeda, N. Sakamoto, T. Ikeda, H. Ohtsuka, A. Xiong, D. Lu, M. Kanehara, T. Teranishi and K. Domen, *Chem. – Eur. J.*, 2010, **16**, 7750–7759.
29 K. Maeda, K. Teramura, D. Lu, T. Takata, N. Saito, Y. Inoue and K. Domen, *Nature*, 2006, **440**, 295.
30 K. Maeda, K. Teramura, H. Masuda, T. Takata, N. Saito, Y. Inoue and K. Domen, *J. Phys. Chem. B*, 2006, **110**, 13107–13112.
31 K. Maeda, K. Teramura, D. Lu, T. Takata, N. Saito, Y. Inoue and K. Domen, *J. Phys. Chem. B*, 2006, **110**, 13753–13758.
32 K. Maeda, A. Xiong, T. Yoshinaga, T. Ikeda, N. Sakamoto, T. Hisatomi, M. Takashima, D. Lu, M. Kanehara, T. Setoyama, T. Teranishi and K. Domen, *Angew. Chem., Int. Ed.*, 2010, **49**, 4096–4099.
33 T. Takata, J. Jiang, Y. Sakata, M. Nakabayashi, N. Shibata, V. Nandal, K. Seki, T. Hisatomi and K. Domen, *Nature*, 2020, **581**, 411–414.
34 K. Maeda, D. Lu and K. Domen, *Chem. – Eur. J.*, 2013, **19**, 4986–4991.
35 K. Maeda and K. Domen, *J. Phys. Chem. Lett.*, 2010, **1**, 2655–2661.
36 J. Soldat, G. W. Busser, M. Muhler and M. Wark, *ChemCatChem*, 2016, **8**, 153–156.
37 K. E. Sanwald, T. F. Berto, A. Jentys, D. M. Camaioni, O. Y. Gutiérrez and J. A. Lercher, *ACS Catal.*, 2018, **8**, 2902–2913.
38 M. Qureshi, T. Shinagawa, N. Tsiapis and K. Takanabe, *ACS Sustainable Chem. Eng.*, 2017, **5**, 8079–8088.
39 R. Pang, K. Teramura, H. Tatsumi, H. Asakura, S. Hosokawa and T. Tanaka, *Chem. Commun.*, 2018, **54**, 1053–1056.
40 B. Tian, W. Gao, X. Zhang, Y. Wu and G. Lu, *Appl. Catal., B*, 2018, **221**, 618–625.
41 Z. Li, F. Zhang, J. Han, J. Zhu, M. Li, B. Zhang, W. Fan, J. Lu and C. Li, *Catal. Lett.*, 2018, **148**, 933–939.
42 G. W. Busser, B. Mei, P. Weide, P. C. K. Vesborg, K. Stührenberg, M. Bauer, X. Huang, M.-G. Willinger, I. Chorkendorff, R. Schlögl and M. Muhler, *ACS Catal.*, 2015, **5**, 5530–5539.
43 J. A. Bau and K. Takanabe, *ACS Catal.*, 2017, **7**, 7931–7940.
44 A. A.-O. X. Garcia-Esparza, T. A.-O. Shinagawa, S. A.-O. Ould-Chikh, M. Qureshi, X. Peng, N. Wei, D. H. Anjum, A. Clo, T. C. Weng, D. Nordlund, D. Sokaras, J. Kubota, K. Domen and K. A.-O. Takanabe, *Angew. Chem., Int. Ed.*, 2017, **56**(21), 5780–5784, DOI: 10.1002/anie.201701861.
45 T. Takata, C. Pan, M. Nakabayashi, N. Shibata and K. Domen, *J. Am. Chem. Soc.*, 2015, **137**, 9627–9634.
46 M. Yoshida, K. Maeda, D. Lu, J. Kubota and K. Domen, *J. Phys. Chem. C*, 2013, **117**, 14000–14006.
47 K. Konishi, in *Gold Clusters, Colloids and Nanoparticles I*, ed. D. M. P. Mingos, Springer International Publishing, Cham, 2014, DOI: 10.1007/430_2014_143, pp. 49–86.
48 F. Wen, U. Englert, B. Gutrath and U. Simon, *Eur. J. Inorg. Chem.*, 2008, 106–111.
49 A. S. Alotabi, Y. Yin, A. Redaa, S. Tesana, G. F. Metha and G. G. Andersson, *J. Chem. Phys.*, 2021, **155**, 164702.
50 R. G. Acres, A. V. Ellis, J. Alvino, C. E. Lenahan, D. A. Khodakov, G. F. Metha and G. G. Andersson, *J. Phys. Chem. C*, 2012, **116**, 6289–6297.
51 D. Briggs, *Auger and X-Ray Photoelecton Spectroscory*, 1990, 1, 151–152.
52 I. M. Band, Y. I. Kharitonov and M. B. Trzhaskovskaya, *At. Data Nucl. Data Tables*, 1979, **23**, 443–505.
53 D. P. Anderson, J. F. Alvino, A. Gentleman, H. Al Qahtani, L. Thomsen, M. I. Polson, G. F. Metha, V. B. Golovko and G. G. Andersson, *Phys. Chem. Chem. Phys.*, 2013, **15**, 3917–3929.
54 D. P. Anderson, R. H. Adnan, J. F. Alvino, O. Shipper, B. Donoeva, J.-Y. Ruzicka, H. Al Qahtani, H. H. Harris, B. Cowie and J. B. Aitken, *Phys. Chem. Chem. Phys.*, 2013, **15**, 14806–14813.
55 J.-Y. Ruzicka, F. Abu Bakar, C. Hoeck, R. Adnan, C. McNicoll, T. Kemmitt, B. C. Cowie, G. F. Metha, G. G. Andersson and V. B. Golovko, *J. Phys. Chem. C*, 2015, **119**, 24465–24474.
56 H. S. Al Qahtani, K. Kimoto, T. Bennett, J. F. Alvino, G. G. Andersson, G. F. Metha, V. B. Golovko, T. Sasaki and T. Nakayama, *J. Chem. Phys.*, 2016, **144**, 114703.
57 H. S. Al Qahtani, G. F. Metha, R. B. Walsh, V. B. Golovko, G. G. Andersson and T. Nakayama, *J. Phys. Chem. C*, 2017, **121**, 10781–10789.
58 S. Zong, L. Tian, X. Guan, C. Cheng, J. Shi and L. Guo, *J. Colloid Interface Sci.*, 2022, **606**, 491–499.
59 A. S. Alotabi, C. T. Gibson, G. F. Metha and G. G. Andersson, *ACS Appl. Energy Mater.*, 2021, **4**, 322–330.
60 J. F. Moulder, *Handbook of X-ray photoelectron spectroscopy*, 1995.
61 H. Mousavi, Y. Yin, L. Howard-Fabretto, S. K. Sharma, V. Golovko, G. G. Andersson, C. J. Shearer and G. F. Metha, *Nanoscale Adv.*, 2021, **3**, 1422–1430.
62 W. Jianjun and X. Qunji, *Wear*, 1994, **176**, 213–216.

© 2022 The Author(s). Published by the Royal Society of Chemistry